Effect of SO_2, O_2, NO_2, and H_2O concentrations on chemical reactions and corrosion of carbon steel in dense phase CO_2.

Bjørn H. Morland[†,1,2], *Truls Norby*[1], *Morten Tjelta*[2], *and Gaute Svenningsen*[2]

Article history:

Received Day Month Year
Accepted Day Month Year
Available Day Month Year

Keywords:

A. CO_2 corrosion
B. Iron sulphate
C. Dense phase CO_2
D. Impurities
E. NO_2
F. SO_2

1 University of Oslo, Department of Chemistry, FERMiO, Gaustadalléen 21, NO-0349 Oslo, Norway.

2 Corrosion Technology department, Instituttveien 18, 2007 Kjeller, Norway.

†Corresponding author: Email: bjorn.morland@ife.no.

ABSTRACT

Carbon capture, utilization and storage (CCUS) is expected to be important method for reducing the CO_2 emissions to prevent global warming. Several species could follow the CO_2 through the capture plant as carry over. It is expected that nitrogen dioxide (NO_2), sulphur dioxide (SO_2), oxygen (O_2), and water (H_2O) can be present as impurities (concentrations at the ppmv level) in the captured CO_2. The exact composition will depend on the flue gas type, the CO_2 capturing process and multiple other parameters. Some of these impurities are reactive and may cause corrosion in carbon steel pipelines and could therefore be a threat for safe CO_2 transport.

The present study used a novel experimental setup to realistically simulate a CO_2 transport pipeline system with a controlled and variable concentration of impurities at a total pressure of 100 bar and a temperature of 25 °C. The water concentration was increased and decreased with constant concentration of SO_2 and O_2, to observe and identify possible reactions or threshold levels which could give corrosion. A similar experiment was conducted with NO_2. First, experiments were carried out without steel coupons, to observe un-catalysed reactions, and then with coupons to measure corrosion rates. The first sign of corrosion appeared at 350 ppmv of water with NO_2 present. At 670 ppmv water with 75 ppmv NO_2 the overall corrosion rate was about 0.57 mm/y and the main product was iron oxide. The corrosion process for SO_2, O_2, and water was much slower, and the first sign of corrosion appeared around 1900 ppmv of water, with about 75 ppmv of SO_2 and 230 ppmv of O_2. The corrosion rate increased some when the water concentration was increased to 2400 ppmv, but the overall corrosion rate was only 3.6 µm/y and the main product on the surface was iron sulphate.

INTRODUCTION

Carbon capture, utilization and storage (CCUS) is needed to meet the goal set by the International Energy Agency (IEA)[1] and the Intergovernmental Panel on Climate Change (IPCC)[2] of limiting the long-term global temperature rise. It will be essential that the cost of the CCUS processes is kept as low as practically possible to achieve the goal. For this reason, carbon steel is most economically feasible material for long transport pipelines. Even if carbon steel is an attractive material for constructing pipelines for transport of dense phase CO_2, not to mention network of pipelines already in place from oil and gas production, it may corrode if the captured CO_2 contains certain combinations of additional species (impurities), especially liquid water. If the water is completely dissolved in the dense phase CO_2, the corrosion rate would be very low, typically around 1 µm/y.[3] Presence of certain species together with water, may increase the corrosion rate and change the type of corrosion products. In the suggested specifications for CO_2 transport,[4, 5] the maximum allowed limit for several impurities like NO_2, SO_2, and H_2S were set for health, safety, and environmental reasons, without considering possible corrosion reactions. Previous work by the authors has shown that water, NO_2, SO_2 , H_2S, and O_2 impurities can react and create an aqueous phase that contains sulphuric and nitric acid.[6]

Even if most CO_2 transport system will not have liquid water present, some water is expected to be present at a concentration well below the solubility limit. This low level of water is probably sufficient to create a thin surface layer (some monolayers) of water at the metal surface. It is known that both SO_2 and NO_2 dissolve in a liquid water phase to form acid. However, reactions in bulk water phase may be different from reactions in thin water films, and it is not known if these acids can form in thin surface layers or if there is a critical layer thickness before the reactions can occur (like in atmospheric corrosion where the adsorbed water reaches the properties of bulk water when the relative humidity exceeds 60 – 70% [7]).

Corrosion and chemical reactions in dense phase CO_2 have been investigated in some experiments with single or multiple impurities. Halseid et al. summarized most of the experiments up to 2014 in a review.[8] There is only a limited number of papers addressing CO_2-H_2O-NO_2 systems, but Dugstad et al.[9] reported corrosion rates of carbon steel from 0.2 up to 1.7 mm/y, depending on the concentration of dissolved water. It was however emphasized that the corrosion rate could be higher due to consumption of the impurities in the corrosion process, meaning that the concentration of the impurities was significantly lower or zero in the end of the experiments. Paschke et al. executed a series of experiments with multiple impurities among other NO and they conclude that the corrosion rate was lower than 80 µm/y as long as the water concentration was less than 1000 ppmv.[10] Several papers address CO_2-H_2O-SO_2 systems, and wide range of corrosion rates from 0.005 to 7 mm/y have been reported[11-20] depending on the concentration of impurities, temperature, flow, and exposure time. Hua et al.[19] indicated that the critical water content with SO_2/O_2 present should be no higher than about 500 ppmv (mole) to minimize localized corrosion attacks, while for avoiding general corrosion rates in excess of 0.1 mm/y the water content should be less than 1900 ppmv. These findings are in

contrast to the findings of Morland et al.[3] who reported rates as low as 1 µm/y even when the solubility limits of water was exceeded for a short period without SO_2/O_2. High localized corrosion rates were also reported by Farelas et al.,[20] which measured 2.4 and 6.8 mm/y at 25 °C (80 bar) in dense phase CO_2 with 650 ppmv water, and 0.05% and 0.1% SO_2, respectively. Water-saturated experiments in general report higher corrosion rates compared to dissolved water experiments. Sun et al. performed several test series[21-24] with water-saturated conditions and multiple impurities. For CO_2-H_2O-SO_2 they reported 0.5 mm/y and the addition of O_2 increased the corrosion rate to 1.0 mm/y. One experimental weakness with the previously reported results is how dissolved and liquid water is introduced into the test system. In most cases the "dissolved" water was introduced as a single quantity of liquid water that, if assuming full mixing with the CO_2 bulk phase, would give a certain water content. However, none of the papers studied the time for such dissolution, but indication of long dissolution time is found in the work from Thodla and Ayello.[25, 26] It was not considered that liquid water droplet could wet the corrosion coupons when water/CO_2 was injected, or if water condensation occurred during depressurization after the experiment was finished.

The objective of this study was to study chemical reactions in between impurities, and corrosion in a simulated CO_2 transport system. To realistically mimic the conditions in transport pipeline, the impurities were introduced as separate CO_2 streams with fully dissolved impurities. The possibility of accidental water deposits on the corrosion coupons was therefore eliminated. Focus was put on identifying which concentration of water that is needed to initiate corrosion and how the corrosion product evolves on the surface.

EXPERIMENTAL PROCEDURE

A transparent autoclave with an internal volume of 0.330 L (Figure 1) was used in these experiments, where windows allowed for in-situ visual observation. The autoclave body was made of 316 stainless steel and the transparent windows consisted of soda lime glass (exposed to the CO_2 phase) and polycarbonate plates (exposed to air) which acted as pressure support for the lime glass. An external magnetic stirrer and an internal magnet was used for mechanical mixing inside the autoclave. Two of the experiments were carried out with corrosion coupons exposed inside the autoclave. The coupon holder was made of polyether ether ketone (PEEK) and could hold three coupons (Figure 2). Still-pictures were taken at regular intervals, one image every 10 minutes. The pictures were used to create a time-lapse video showing the experimental development. A LED-lamp was used to achieve constant light conditions.

High precision piston pumps (0.266 L volume) from Teledyne, containing pre-mixed solutions of CO_2 and the respective impurities, were for controlled injection. The piston pump was pressurized slightly above 10 MPa to prevent backflow. Impurity injection was carried out through individual 1/16" tubing that ended up inside the autoclave (see Figure 2). In addition, pure CO_2 (99.999%) with H_2O was also injected to the autoclave from a booster pump. A liquid pressure regulator was used to keep the autoclave at a constant pressure of 10 MPa. The flow ratio for impurity pump versus booster pump was about 1:50. If the piston pump was stopped, the pure CO_2 flow from the booster pump would increase the flow automatically to maintain the pressure and the same total flow rate. The piston pump was filled with stock solutions containing about 20 times higher impurity concentrations than the desired test concentration. Thus, the concentration at the tip of the injection tube was higher before the stream was mixed (diluted) with the rest of the autoclave volume.

Water was introduced by forcing a CO_2 slip stream through a cylinder with liquid water, which gave near fully water saturated CO_2 without liquid water. The water content of the bulk CO_2 could be adjusted from bottle dry to near full saturation by adjusting the ratio between the dry CO_2 flow and the water saturated CO_2 flow. The slip stream flow was controlled by using a mini Cori-flow controller from Bronkhorst. These streams were mixed before the autoclave, ensuring that the water always was completely dissolved in the CO_2 before the stream entered the autoclave. Thus, no liquid water was introduced to the system. However, liquid water did form inside the autoclave when it was cooled down to force the system to exceed the water solubility limit in CO_2.

The pressure of the exhaust CO_2 was reduced from 10 to 0.2 MPa in a heated vaporizing regulator (to avoid precipitation of impurities and hydrate formation). The low-pressure gas was routed to the analysing module which consisted of two multicomponent laser spectrographs in series: ap2e (ProCeas) and one Emerson (CT5400). None of the analysers could handle a pressure of 10 MPa, which is why the pressure had to be reduced to about 0.2 MPa prior to the analysis and the measurements was performed at ambient pressure. At ambient pressure, ppm volume equals ppm mole. So, even when the pressure in the experiment was 10 MPa, the reported ppmv concentration is in fact ppm mole. The volume in ppmv must not be mistaken as the volume related to the liquid CO_2 or the autoclave. The total flow through the system was about 1 g/min and it was controlled by a Bronkhorst mass flow controller at the low-pressure side. It was possible to route the individual impurity streams around the autoclave and send them directly to the analyser module. Thus, possible consumption of impurities could be detected by measuring the difference in inlet and outlet concentrations. The accuracy of the analysers was about 1 percent of the full scale, which amount to about ±1 ppmv for SO_2 and NO_2. While H_2O and O_2 had an accuracy of ±3 ppmv., since the measurements was performed at ambient pressure. There will always be some uneven measurements of the exhaust gas since diurnal temperature changes will affect the density of the CO_2 in the reservoir tank and in this way either increase or decrease the amount of impurities entering the autoclave. To reduce the diurnal effects, the whole system was placed inside a temperature-controlled room, but small fluctuations still occurred (about ±0.3 °C). These small changes in room temperature resulted in small fluctuations in the measured concentrations (about 1.5 % from the set value over a period of 24 hours). This means that periodic fluctuations over 24 hours are attributed to temperature effects and are not caused by reactions.

Four experiments were performed. Two of the experiments were carried out to only study possible chemical reactions and did therefore not include corrosion coupons. The two other experiments had three different types of corrosion coupons: carbon steel with polished surfaces, carbon steel with mill scale, and duplex stainless steel (1.4462). The latter two was added as a screening test and to observe if the original mill scale could give some protection. The experimental conditions are summarized in Table 1.

The start and stop procedure was as follows: After the coupon holder had been mounted (if present) inside the autoclave, it was first purged with low pressure CO_2 (0.3 MPa for 30 minutes) and then high-pressure CO_2 (10 MPa for about 20 minutes), to remove air and moisture from the system. The water concentration was usually about 50 ppmv after this purging process. Further two days of CO_2 purging at 1 g/min was needed to reach a water content as low as 10 ppmv. When the experiment was finished, the feed was shifted to only dry CO_2 to remove impurities and avoid uncontrolled precipitation (water, reaction products) during depressurisation.

The carbon steel coupons used in Experiment 02 and Experiment 04 (called Exp-02 and Exp-04) were S355MC grade (1.0976) with the

composition given in Table 2. One of the three coupons had a pre-made mill scale surface layer. In Exp-02 the mill scale was 5 wt.% wüstite and 95 wt.% magnetite, while in Exp-04 the mill scale was 70 wt.% wüstite and 30 wt.% magnetite. The size of all corrosion coupons were 9.55 x 9.55 mm. The polished carbon steel coupons were 4 mm thick, while the coupon with mill scale and the duplex coupon were 3 mm thick. All sides (surfaces) of the coupons, including the side walls, were exposed in the experiments.

The gas qualities that were used to make pre-mixed solutions of CO_2 are listed in Table 3.

Corrosion products were removed using chemical stripping in Clarke's solution (inhibited HCl solution) and the weight loss was determined according to ASTM G1-90.

RESULTS AND DISCUSSION

Experiments with SO_2 and O_2 (Exp-01 and Exp-02)

The results from the first experiment are shown in Figure 3. Both water and SO_2/O_2 concentrations were increased in steps, and at the end of the experiment the temperature was lowered to force the system to exceed the water solubility limit. For the current condition (10 MPa and 25 °C) the water solubility limit is 3200 ppmv in a pure CO_2-H_2O system.[4] The concentration of the SO_2/O_2 and H_2O was increased multiple times to observe if any reactions would start as the concentration of the impurities increased in the autoclave. A positive sign of a chemical reaction would be either a significant change in one or more impurity concentration in the exhaust gas, or visual observation of reactions/reaction products inside the autoclave. Since O_2 and SO_2 were injected by the same pump, the ratio between them in the exhaust gas should be the same as long as no reactions occurred. A pressure decrease or change in injection rate would affect the concentrations in terms of absolute values but not the concentration ratio.

In Exp-01, the water content was increased six times (red line, Figure 3), starting at 10 ppmv up to 2800 ppmv, and at the end exceeding the water solubility limit due to reduced temperature. The SO_2 and O_2 concentrations were also increased multiple times throughout the experiment (blue and black line, Figure 3), starting at about 10 ppmv SO_2 and 20 ppmv O_2, and ending at about 100 ppmv SO_2 and 220 ppmv O_2. Except for some small intermittent transients, the gas analysis gave no indications of reactions taking place. Fluctuations, which were most clear on the highest concentrations, were related to diurnal temperature changes. The first decrease in SO_2 and O_2 concentration occurred when the water concentration increased from 50 to 130 ppmv (at 60 hours). However, the concentration went back to their original levels, indicating that this was only a transient occurrence. The same could be observed at a larger scale at 350 hours when the temperature was reduced from 25 to 6 °C. The reason for this decrease is believed not to be reactions, but rather an effect related to density changes during cooling of the liquid CO_2. Reduced density will require more CO_2 from the booster pump, to prevent a pressure drop, and will therefore intermittently give higher dilution of the impurities which are injected at a constant rate. As the temperature and the density stabilized, the concentration of SO_2 and O_2 reverted to their original levels.

During the cooling period (352 – 400 hours), the H_2O concentration dropped from 2700 ppmv to about 1900 ppmv and remained stable, indicating that the solubility limit was exceeded, and that water precipitated inside the autoclave. Even though the water solubility limit was exceeded, no decrease in SO_2 and O_2 concentrations was observed from the gas analysis.

The second experiment, Exp-02, was carried out with corrosion coupons, and the SO_2 and O_2 contents were kept constant and only water was increased (Figure 4). A leakage in the cap sealing of the injection pump caused a drop in the SO_2 and O_2 concentrations in the 80 – 300 hours period. The pump sealing was replaced at 330 hours, but still there was a minor leakage. The pressure inside the autoclave was not affected by the pump problems, nor the temperature, since the system was closed while the sealing was replaced.

Because of this leakage, it was difficult to conclude if the concentration of SO_2 or O_2 did decrease due to reactions or due to the diurnal fluctuations during the first 400 hours. However, the SO_2 / O_2 ratio remained constant during this period (not shown), indicating that no reactions occurred. The pictures taken during the experiment in this period (Figure 5a - c), showed no change on the surface of the coupons. However, after the last increment of H_2O at 476 hours, the slope of the decreasing SO_2 and O_2 concentration was different as seen in Figure 4b, indicating some consumption of these impurities. The pictures showed that the surface of both the mill scale (left, Figure 5d) and the carbon steel coupon (right, Figure 5d) turned grey during this period. Enlargement of the carbon steel coupon is shown in Figure 6. To increase the sensitivity of impurities consumption and possible reactions, the autoclave was closed from 550 hours to 635 hours, while the feed of CO_2 and impurities was by-passed the autoclave but otherwise kept unchanged. There were no compositional changes observed when the autoclave was opened again.

Injection of water and impurities was stopped at 658 hours, and only pure CO_2 was purged through the autoclave before the experiment was stopped. The exposed corrosion coupons were examined in Scanning Electron Microscope (SEM), and uniformly spread globular products were identified on the surface (Figure 7) of the carbon steel coupons. Energy-dispersive X-ray spectroscopy (EDS) analysis showed that the surface product contained Fe, S and O, with a compositional ratio that matched relatively well with $FeSO_4$ (point 4, 5, 6, and 7 in Figure 7). Examination with X-ray diffraction (XRD), gave no clear results, indicating that the products were amorphous or too thin to analyze.

The weight loss of the polished carbon steel coupon was 0.2 mg/cm^2, this corresponding to an average corrosion rate of 3.6 µm/y throughout the experiment, or 8.5 µm/y if only the period with observed surface change is considered.

Experiments with NO_2 and H_2O (Exp-03 and Exp-04)

Two experiments were performed with NO_2 and H_2O. In both experiments the NO_2 content was kept constant while the H_2O concentration was increased in steps. Only one experiment (Exp-04) had corrosion coupons.

Due to diurnal temperature changes, there were some fluctuations of the NO_2 concentration in these experiments. The injection pump needed to be refilled several times, and the concentration was slightly different in each batch. Therefore, the concentration changes should be identified within the same blend in the pump, as indicated with different shading in Figure 8.

The gas analysis in Exp-03 showed no real changes in the NO_2 concentration in the first period when the water concentration was increased from zero to about 1300 ppmv (Figure 8). There was some small permanent change in the average NO_2 concentration when the water concentration was stable in-between the increase and decrease periods above 1300 ppmv of H_2O. This could indicate consumption of NO_2 due to reaction. However, the fluctuation made it difficult to make this conclusion with confidence. Interestingly, the NO_2 concentration

always decreased intermittently when the water concentration was increased to maximum water concentration (Figure 8, 160 to 200 hours, 520 to 560 hours, and 760 to 780 hours), and the opposite occurred when the water concentration was decreased from maximum at 270, 608, and 810 hours. The "NO_2 increase periods" was much shorter than the "NO_2 decrease periods", but the integrated area between the injected and analysed concentration level was the same for both periods (not shown).

In the second NO_2 experiment, Exp-04, corrosion coupons were present. As before, the NO_2 concentration was kept stable while the water concentration was increased (Figure 9).

After the water content had been increased from 30 ppmv to about 350 ppmv (Figure 9, after 72 hours), the carbon steel coupon gradually became darker and stained, but the process was slow. At 168 hours the water concentration was increased to about 670 ppmv. Immediately after, the color of the carbon steel coupon started to change, and black spots started to appear (Figure 10c and Figure 11c). With time the black spots gradually turned brown, and in the end the whole coupon was cowered with a brown surface product. Since no clear consumption was observed from the gas analysis, the autoclave was closed from 377 to 459 hours, to increase the sensitivity for the gas analysis if the reaction process was slow. When the autoclave was opened again, water and NO_2 had decreased by 16 ppmv and 35 ppmv, respectively, while NO had increased with 12 ppmv.

The duplex stainless-steel coupon was unaffected by the exposure. The mill scale coupon was covered with corrosion products on the ground sides (where the mill scale had been removed), and on mechanical cracks in the mill scale (these cracks were formed during machining, before exposure).

On both carbon steel coupons (with and without mill scale), the brown products were loosely adhered and fell off easily, exposing a darker layer underneath. SEM and EDS analysis (Figure 12) revealed that the surface products consisted mainly of Fe and O with smaller amounts of C and Mn. Al was also detected, but this was an artefact from the sample holder that was made of aluminum. The surface products were most likely iron oxide, and variations in the Fe:O ratio suggests that several types were present. However, due to overlapping peaks in the EDS spectra it was not possible to clarify if the corrosion products also contained N (nitrogen).

When the surface products were removed chemically with Clarke's inhibited HCl solution, the weight loss was 26.7 mg/cm², which gives an average corrosion rate of 0.57 mm/y for the whole experiments duration.

Discussion of the results

It was difficult to identify chemical reactions from the gas analysis alone since the diurnal fluctuations may have overshadowed small impurity consumptions due to reactions. The SO_2-O_2 experiment without steel coupons (Exp-01, Figure 3), did not show any clear sign of decrease or increase of the impurities due to reaction or absorption when the water concentration was increased. Even when the water solubility limit was exceeded, the SO_2 and O_2 concentration remained at the injected level. However, with NO_2 and water (Exp-03, Figure 8) there were several intermittent periods where NO_2 either increased or decreased with the change of water concentration, as shown in detail in Figure 13. When the water concentration increased, the NO_2 decreased temporary, while NO_2 increased temporary when the water concentration decreased. This effect was more pronounced with water concentration above 1300 ppmv. This phenomenon is most likely related to NO_2 absorption or adsorption in thin water layers (i.e. an unknown number of "monolayers") on surfaces inside the autoclave, as discussed by Nelli et al.[27, 28] It could be argued that this might just be reaction with water to produce another species that was not analysed for, like nitric acid or one of many type of nitrogen oxides, in the CO_2 phase. If so, the effect should be permeant and not temporary as seen here. Integration of the decrease, around 178 h, showed that about 0.53 mmol of NO_2 disappeared while during the increase around 268 h about 0.50 mmol NO_2 appeared, i.e. the increase and decrease were essentially of similar size. The thickness of the water layer will increase with increasing dissolved water content and thereby allow more NO_2 to absorb, and vice versa, less dissolved water content will reduce the water layer thickness and reduce the amount of "dissolved" NO_2. According to atmospheric corrosion theory the surface water layer will at some point reach a critical thickness where it approaches bulk water properties,[29] typically around 60 to 80% of relative humidity (RH) in air. This corresponds to about three to five monolayers of surface water.[30] For iron in air, the critical RH where corrosion starts is around 60% RH, and there is a sharp increase in corrosion rate when the RH passes 75-80% RH.[7] Even though humid air and dense phase CO_2 are quite different, and the relationship between water content and water surface layer thickness is not known, it may be assumed that the principles are similar. For comparison, 1300 ppmv water dissolved in CO_2 would be equal about 40% RH, relative to the solubility limit of water in CO_2 at 25 °C which is about 3200 ppmv at 10 MPa.[4] A water content of 2400 ppmv would then be equivalent with 75% RH, for which the water film is reported to have near bulk water properties in air.[29] Thus, the observed intermittent decrease/increase of NO_2 could simply be related to thickness changes of the thin water surface film. This fits qualitatively well with the analysis shown in Figure 13. The geometric surface area inside the autoclave and the tubing amounts to about 640 cm^2, and the measured decrease in NO_2 concentration amounts to about 4E+17 molecules per cm^2. The surface roughness is unknown but would contribute considerably to increase the specific surface area, especially in the tubing. This would give a lower number of molecules per cm^2. The number of water molecules in a monolayer at ambient pressure in air is reported to be about 2E+16 molecules per cm^2.[31] Assuming that NO_2 binds with water in the ratio of 2:1 to form HNO_3 and HNO_2 at the metal surfaces,[32, 33] only a few monolayers of water is needed to achieve this ratio. Most likely the process is completely reversible if no other reactions take place, i.e. if there is no corrosion. These observations indicate that SO_2 and NO_2 exhibit different properties in CO_2 with dissolved water, which became even clearer when carbon steel coupons were introduced.

The SO_2-O_2-H_2O experiment with corrosion coupons (Exp-02, Figure 4) showed that the water concentration had to be 1900 ppmv before the carbon steel coupon showed visual sign of reaction on the surface. The surface appearance changed slightly when the water was increased to about 2400 ppmv. This suggests that SO_2 needs a certain amount of water, or the water needs to have near bulk water properties on the surface of the metal, for the SO_2 to absorb and create sulphurous and sulphuric acid. Only then can the corrosion of carbon steel start and products form on the surface. The process appears to be slow, with a corrosion rate of only 3.6 µm/y (average for the whole experiment). Possibly, the initial corrosion products could act as a barrier that slowed down further corrosion. There were no indications that SO_2 and H_2O reacted in the bulk CO_2 to form H_2SO_3 (or H_2SO_4) which later condensed on the surface of the carbon steel, since the deposits evolved uniformly on the carbon steel coupons. In-house data produced within the Kjeller dense phase project, (to be published later) has shown that the solubility of H_2SO_4 is about 1 ppmv in dense phase CO_2 at 100 bar and 25 °C. If this concentration was exceeded, H_2SO_4 would start to precipitate inside the autoclave, which there was no visible sign of. There could of course be a threshold value for SO_2, water or both to form H_2SO_4 freely in the CO_2. Since the water was already close to the

solubility limit, the threshold value for forming acid should depend on the SO_2 concentration. The current experiments were mainly conducted at 25 °C, and it could be expected that condensation would occur at a lower temperature. However, in Exp-01 (Figure 3) the temperature was lowered to 6 °C towards the end of the experiment and no immediately condensation started. After 50 hours at 6 °C, the wet CO_2 line clogged due to hydrate formation and the CO_2 feed was stopped while the temperature and pressure was maintained. During these 50 hours with 6 °C, no precipitation was observed inside the autoclave, indicating that H_2SO_3 or H_2SO_4 will not form in the CO_2 bulk phase with 90 ppmv of SO_2, even at the solubility limit for water in CO_2. It is therefore concluded that the corrosion process is dependent on absorption of SO_2 into the thin water film on the steel surface. The latter is supported by atmospheric corrosion theory,[30] where absorption of species in water films can promote corrosion.

The NO_2-H_2O experiment (Exp-04, Figure 9) with carbon steel showed clearly that reactions on the surface of the carbon steel coupon occurred with a water content as low as 350 ppmv, but even after 100 hours the coupon was just partly covered showing that the discoloration of the surface was very slow. The apparent corrosion rate, as judged from over 1000 of pictures, increased when the water content was increased to 670 ppmv. From the moment the water content was increased, at 169 hours, to the point when the carbon steel coupon appeared to be completely covered, it took only 8 hours and the water concentration was at this time 594 ppmv (Figure 14a-e). At 179 hours, a slightly darker surface product was observed, and it gradually evolved (Figure 14f-i) until the corrosion increases at 187 hours and dark spots appears.

The phenomenon when the surface goes from partial to full coverage of corrosion products, which occurred between 169 – 177 hours, has been observed previously in a system with only CO_2 and water.[3] When the water solubility limit was exceeded the carbon steel coupon started to change colour. It was concluded that the colour change was caused by formation of $FeCO_3$ when the surface water film was thick enough to get the corrosion process started, which happened at a water content of 2400 ppmv at 14 °C. SO_2 is considered 10 times more soluble than NO_2 in water films[34, 35] and Oesch et al. reported about 4 times higher corrosion rate with 10 ppmv SO_2 compared to 10 ppmv NO_2 (although in air, 90% RH). These observations are opposite of what was observed in the present work. The first sign of surface products in the SO_2-O_2-H_2O-system appeared at 1900 ppmv of water while for the NO_2-H_2O-system it was observed with only 350 ppmv of water. This indicates that another mechanism enhances the corrosion process for NO_2-H_2O-system in dense phase CO_2. It is assumed that the water solubility in CO_2 was not significantly affected by the presence of NO_2 in these experiments, since no precipitation was observed in Exp-03 with a water concentration of 2400 ppmv. The phenomenon could be a combination of first adsorption of NO_2 and H_2O to the surface of the carbon steel, formation of thin water film, and then absorption of NO_2 in this surface water film. There are many studies about the adsorption and surface reaction processes of NO_2 on solid surfaces in air, but the number of studies on iron is limited,[35-37] and no studies has been found for dense phase CO_2. Details about the reactions between the steel substrate, water film and NO_2 is not known in dense phase CO_2, but adsorption directly on the steel substrate cannot be ruled out. The route from adsorption of NO_2 to corrosive media on the surface of the carbon steel is very complex, but it is known that surface hydroxy groups together with NO_2 is a strongly hydrophilic molecule which can attract more water to the surface and replace the surface OH groups by NO_3^-.[38] This could be the process observed in the beginning of the depositing on the carbon steel up to 169 hours, where only cluster-like products were visible. The adsorbed NO_2 and produced NO_3^- might then promote further water transport (through absorption, chemisorption) to the surface film. At some point, the corrosion of the steel substrate will accelerate, as seen when the water concentration was increased to 670 ppmv in Exp-04. If the corrosion product is hygroscopic, it will promote further water transport to the surface film. It was shown that 350 ppmv water in the CO_2 bulk resulted in partly coverage of the carbon steel surface while 500 to 600 ppmv of water gave full coverage of corrosion products. The second change of surfaces (Figure 14f–i) that was present before the black spots appeared (at 187 hours) might indicate that the surface water film had reached a thickness which allowed corrosion processes to fully start, and that the corrosion process became self-driven when the water content was 670 ppmv. It is likely that some of the dissolved NO_2 will react with water and form acids and NO, which is supported by the fact that the NO concentration increased slightly with increasing water concentration in Exp-04 (Figure 9). In the period where the autoclave was closed (from 377 to 459 hours) the reduction of NO_2 was 35 ppmv and the increase of NO was 12 ppmv, giving a ratio of 3:1. This is in agreement with the overall reaction to produce nitric acid from NO_2 and water:[27]

$$3NO_2(g) + H_2O(l) \rightarrow 2HNO_3(l) + NO(g) \quad (1)$$

Sim et al.[39] used potentiodynamic polarization tests and found that for the same molar concentration in a large water phase, HNO_3 was about twice as corrosive as H_2SO_4 with gaseous CO_2 present. This cannot explain the 100-fold difference in corrosion rate were found in the present work, but it does support an additional or enhanced mechanism acting for NO_2-H_2O-systems in dense phase CO_2. The main product on the carbon steel coupon in Exp-04 was iron oxide. The exact type of iron oxide could not be identified, and nitrates could also be present. Normally, there has been reported iron oxide (FeOOH) when carbon steel is exposed to NO, NO_2, or HNO_3. Samie et al.[40] reported the same when carbon steel was exposed to HNO_3 (in air) and analysed with XRD. However, an analysis with FT-IR showed that iron nitrate was present.

The corrosion rates in the present work were determined by weight loss and total exposure time. Since the conditions were changed during the experiments, the corrosion rates cannot be linked directly to a certain concentration. However, the still pictures gave reliable indications of when there was activity on the surface of the carbon steel coupons. It was therefore possible to exclude periods where corrosion did not occur. The first sign of corrosion was observed after 400 hours in Exp-02 (SO_2-O_2-H_2O) with a water concentration was at about 1900 ppmv, and after 169 hours in Exp-04 (NO_2-H_2O) when the water was about 350 ppmv. This correction of "exposure" time would increase the corrosion rate in Exp-02 from 3.6 µm/y to 8.5 µm/y, while the corrosion rate in Exp-04 increased from 0.57 to 0.67 mm/y. If only the period from the water content was 670 ppmv is used and black spots first appeared, the corrosion rate would increase further to 0.84 mm/y. For a pipeline with an expected lifetime of 50 years this would require a corrosion allowance of 43 mm, which is too high to be acceptable.

The Energy-dispersive X-ray spectroscopy (EDS) indicated that the corrosion products on the carbon steel coupons were $FeSO_4$ (Exp-02) and iron oxide (Exp-04). Some carbon was also found on the coupon in the Exp-04 experiment with NO_2 and water, which could indicate presence of iron carbonate. Further investigation by XRD gave no clear results, indicating that the products were amorphous or too thin to be analysed. Iron oxide was also found on the mill-scale coupon, especially at the sides and in the cracks of the mill scale. This indicates that the mill scale gives good protection, but corrosion may occur if there are cracks present. This was also observed in the experiments with SO_2, O_2, and water (Exp-02). The same spherical $FeSO_4$ product was found at crack sites as on the polished carbon steel coupons, see Figure 15. It was not possible to determine mass loss of the mill scale coupons, due to the stripping process also removed the mill scale.

The same type of spherical $FeSO_4$ products were reported by Hua et al.[19] and Choi et al.[41] However, they concluded based on XRD investigation that the products were $FeSO_3 \cdot 3H_2O$. It could be suggested that these spherical products were formed by precipitation or condensation of micro droplets of H_2SO_4, but no such products were found on the duplex coupon. If acid was condensing onto the surface of carbon steel, it should condense on all surfaces, including the duplex. Since this was not observed by camera or by SEM, it is concluded that no precipitation occurs but instead the spherical products are formed by reactions at the surface of the coupon.

There was no indication of pitting or local attacks on the polish carbon steel coupons. The duplex coupon was not attacked during the experiments.

CONCLUSIONS

Experiments were carried out at 25 °C and 100 bar CO_2 with varying amounts of water and impurities. It was difficult to detect reactions and corrosion of carbon steel only from the gas analyses, but some indication of NO_2 absorption/desorption was observed. There was no observation of SO_2/O_2 reaction or absorption, even when the water solubility in CO_2 was exceeded for a short period. With carbon steel coupons present, products from corrosion reactions could be observed visually even if the gas analysis showed no consumption.

- With 75 ppmv NO_2 present, the corrosion of carbon steel started when the water content reached 350 ppmv and it increased significantly when the water content was increased further to 670 ppmv. The corrosion rate was found to be 0.57 mm/y.
- With 75 ppmv SO_2 and 230 ppmv O_2 present, slight corrosion was observed on carbon steel coupons when the water content was increased to 1900 ppmv. The corrosion rate was found to be 3.6 µm/y.
- The corrosion products, indicated by EDS, was $FeSO_4$ in the SO_2/O_2 experiment and iron oxides in the NO_2 experiment.
- No pitting or localized attacks was found on the polished carbon steel coupons.
- No attacks were observed on the duplex coupons.

ACKNOWLEDGEMENT

The present work was carried out as part of the Kjeller Dense Phase CO_2 Corrosion II project (KDC-II). The authors would like to thank CLIMIT (Norwegian Research Council, project no. 243624/E20), Shell, Total, ArcelorMittal, OLI, and Gassco for financial and technical support.

References

1. IEA, "Energy Technology Perspectives 2010, Scenarios & Strategies to 2050," (Paris, France, 2010).
2. IPCC, "Climate Change 2013: The Physical Science Basis.," (Cambridge University Press, Cambridge, United Kingdom and New York, NY, USA, 2013).
3. B.H. Morland, A. Dugstad, G. Svenningsen, *Energy Procedia* 114, (2017): p. 6752-6765.
4. E. de Visser, C. Hendriks, M. Barrio, M. Mølnvik, G. de Koeijer, S. Liljemark, Y. Le Gallo, *International Journal of Greenhouse Gas Control* 2, (2008): p. 478.
5. S. Herron, P. Myles, "Quality Guidelines for Energy System Studies - Co_2 Impurity Design Parameters," DOE/N/NETL-341/011212, (2013).
6. A. Dugstad, M. Halseid, B. Morland, *Energy Procedia* 63, (2014): p. 2547-2556.
7. S.L. Pohlman, in *Atmospheric Corrosion*, ed., vol. 13 (Metals Park, OH: ASM International, 1987), p. 80-83.
8. M. Halseid, A. Dugstad, B. Morland, *Energy Procedia* 63, (2014): p. 2557-2569.
9. A. Dugstad, M. Halseid, B. Morland, S. Clausen, "Dense Phase Co_2 Transport – When Is Corrosion a Threat," Northern Area Western Conference/2011, (Houston, TX: NACE International, 2011).
10. B. Paschke, A. Kather, *Energy Procedia* 23, (2012): p. 207-215.
11. A. Dugstad, M. Halseid, B. Morland, A.O. Sivertsen, "Corrosion in Dense Phase Co2 with Small Amounts of So2, No2 and Water," (Eurocorr 2012, 2012).
12. A. Dugstad, M. Halseid, B. Morland, *Energy Procedia* 37, (2013): p. 2877-2887.
13. A. Dugstad, M. Halseid, B. Morland, "Corrosion and Solid Formation in Pipelines Transporting Dense Phase Co2 with Impurities – What Do We Know and What We Need to Know," (The 3rd International Forum on the Transportation of CO2, 2012).
14. Y. Xiang, Z. Wang, X. Yang, Z. Li, W. Ni, *The Journal of Supercritical Fluids* 67, (2012): p. 14-21.
15. Y. Xiang, Z. Wang, C. Xu, C. Zhou, Z. Li, W. Ni, *The Journal of Supercritical Fluids* 58, 2 (2011): p. 286-294.
16. Y. Xiang, Z. Wang, Z. Li, W.D. Ni, *Corrosion* 69, 3 (2013): p. 251-258.
17. Y. Xiang, Z. Wang, Z. Li, W.D. Ni, *Corrosion Engineering, Science and Technology* 48, 2 (2013): p. 121-129.
18. F. Farelas, Y.S. Choi, S. Nesic, "Effects of Co2 Phase Change, So2 Content and Flow on the Corrosion of Co2 Transmission Pipeline Steel," CORROSION/2012, paper no. 1322 (Houston, TX: NACE International, 2012).
19. Y. Hua, R. Barker, A. Neville, *International Journal of Greenhouse Gas Control* 37, (2015): p. 412-423.
20. F. Farelas, Y.S. Choi, S. Nesic, *Corrosion* 69, 3 (2012): p. 243-250.
21. C. Sun, J. Sun, S. Liu, Y. Wang, *Corrosion Science* 137, (2018): p. 151-162.
22. C. Sun, J. Sun, Y. Wang, X. Lin, X. Li, X. Cheng, H. Liu, *Corrosion Science* 107, (2016): p. 193-203.
23. C. Sun, Y. Wang, J. Sun, X. Lin, X. Li, H. Liu, X. Cheng, *The Journal of Supercritical Fluids* 116, (2016): p. 70-82.
24. J. Sun, C. Sun, G. Zhang, X. Li, W. Zhao, T. Jiang, H. Liu, X. Cheng, Y. Wang, *Corrosion Science* 107, Supplement C (2016): p. 31-40.
25. R. Thodla, A. Francois, N. Sridhar, "Materials Performance in Supercritical Co2 Environments," CORROSION/2009, paper no. 09255 (Houston, TX: NACE International, 2009).
26. F. Ayello, K. Evans, R. Thodla, N. Sridhar, "Effect of Impurities on Corrosion of Steel in Supercritical Co2," CORROSION/2010, paper no. 10193 (Houston, TX: NACE International, 2010).
27. C.H. Nelli, G.T. Rochelle, *Industrial & Engineering Chemistry Research* 35, 4 (1996): p. 999-1005.
28. C.H. Nelli, G.T. Rochelle, *Journal of the Air Waste Management Association* 48, 9 (1998): p. 819-828.
29. Y. Ben-Da, S. Meilink, G.W. Warren, P. Wynblatt, *Components, Hybrids, and Manufacturing Technology, IEEE Transactions on* 10, 2 (1987): p. 247-251.

30. C. Leygraf, *P. Marcus, J. Oudar (Eds.), Corrosion Mechanisms in Theory and Practice*, (New York: 1995).
31. D. Li, Y. Cheng, Y. Li, L. Zhao, W. Sun, Y. Wang, *Vacuum* 136, (2017): p. 14-19.
32. A. Febo, F. De Santis, C. Perrino, A. Liberti, *Tropospheric NOx Chemistry-Gas Phase and Multiphase Aspects, CEC Air Pollut. Res. Rep* 9, (1987): p. 61-67.
33. F. Sakamaki, S. Hatakeyama, H. Akimoto, *International Journal of Chemical Kinetics* 15, 10 (1983): p. 1013-1029.
34. H. Takeuchi, M. Ando, N. Kizawa, *Industrial Engineering Chemistry Process Design Development* 16, 3 (1977): p. 303-308.
35. C. Arroyave, M. Morcillo, *Corrosion Science* 37, 2 (1995): p. 293-305.
36. H.-L. Chen, S.-Y. Wu, H.-T. Chen, J.-G. Chang, S.-P. Ju, C. Tsai, L.-C. Hsu, *Langmuir* 26, 10 (2010): p. 7157-7164.
37. M. Iwasaki, H. Shinjoh, *Physical Chemistry Chemical Physics* 12, 10 (2010): p. 2365-2372.
38. K.I. Hadjiivanov, D.G. Klissurski, V.P. Bushev, *Journal of the Chemical Society, Faraday Transactions* 91, 1 (1995): p. 149-153.
39. S. Sim, M.K. Cavanaugh, P. Corrigan, I.S. Cole, N. Birbilis, *Corrosion* 69, 5 (2012): p. 477-486.
40. F. Samie, J. Tidblad, V. Kucera, C. Leygraf, *Atmospheric Environment* 41, 23 (2007): p. 4888-4896.
41. Y.-S. Choi, S. Nesic, "Effect of Impurities on the Corrosion Behavior of Carbon Steel in Supercritical Co2 - Water Environments," CORROSION/2010, (Houston, TX: NACE International, 2010).

FIGURE CAPTIONS

FIGURE 1. Photo showing the transparent autoclave with camera and injection tubing.
FIGURE 2. Photo of the autoclave interior with coupon holder and three coupons and the stirring magnet. The impurities were injected through the tubes from the top.
FIGURE 3. Analysis of the exhaust gas from Exp-01. The dashed lines indicate the time for change in temperature, water content or SO_2/O_2 content.
FIGURE 4. Analysis of exhaust gas from Exp-02. The dashed lines indicate events like change in water content or by-pass period.
FIGURE 5. Still images from Exp-02. The left, middle, and right-hand side corrosion coupons were, respectively, carbon steel with mill scale, duplex steel, and polished carbon steel.
FIGURE 6. Enlargement of the polished carbon steel coupon from Figure 5 with time scale.
FIGURE 7. (A) SEM picture and (B and C) EDS analysis (atomic %) of carbon steel coupon exposed in Exp-02.
FIGURE 8. Analysis of exhaust gas in Exp-03. Periods with same impurity batch in the injection pump are indicated as white or light grey areas.
FIGURE 9. Analysis of exhaust gas in Exp-04. The dashed lines indicate the time for change in water content.
FIGURE 10. Still pictures from Exp-04. The left, center, and right-hand side corrosion coupons were, respectively, duplex stainless steel, carbon steel with mill scale, and polished carbon steel.
FIGURE 11. Enlargement of the carbon steel coupon in Figure 10 with time scale, exposed to 70 ppmv NO_2 and max. 670 ppmv water.
FIGURE 12. (A) SEM and (B, C) EDS analysis (atomic %) of carbon steel coupon exposed in Exp-04.
FIGURE 13. Extract from Figure 7 (Exp-03) showing the absorption and desorption of NO_2 with increasing and decreasing water concentration. The dashed lines are theoretical concentrations, made from mass balance calculations assuming that no chemical reactions occurred.
FIGURE 14. Exp-04; The carbon steel coupon exposed to NO_2 with increasing water concentration.
FIGURE 15. Close-up of Figure 6, showing spherical $FeSO_4$ products on the carbon steel surface.

TABLE CAPTIONS

TABLE 1: Experimental matrix.
TABLE 2: Chemical composition of the carbon steel used in Exp-02 and Exp-04. The balance is iron.
TABLE 3: Gas qualities of impurities used in the experiments

Table 1. Experimental matrix.

Experiment	Corrosion coupons	Temperature (°C)	Pressure (bara)	SO_2 (ppmv)	NO_2 (ppmv)	O_2 (ppmv)	H_2O (ppmv)
Ramp01	None	6 - 25	99	10 - 85	0	25 - 215	10 - 2800
Ramp02	Three	25.6	99	70 - 85	0	200 - 240	10 - 1900
Ramp03	None	25.6	100	0	40 - 60	0	20 - 2450
Ramp04	Three	25.7	100	0	70	0	20 - 670

Table 2. Chemical composition of the carbon steel used in Exp-02 and Exp-04. The balance is iron.

Element	C	Si	Mn	P	S	V	Nb	Ti	Al
Wt. %	< 0.12	< 0.5	< 1.5	< 0.025	< 0.02	< 0.2	< 0.09	< 0.15	> 0.015

Table 3. Gas qualities of impurities used in the experiments.

Gas type	Purity, %
CO_2	99.999
NO_2	99
SO_2	99.9
O_2	99.999

FIGURE 1. Photo showing the transparent autoclave with camera and injection tubing.

FIGURE 2. Photo of the autoclave interior with coupon holder and three coupons and the stirring magnet. The impurities were injected through the tubes from the top.

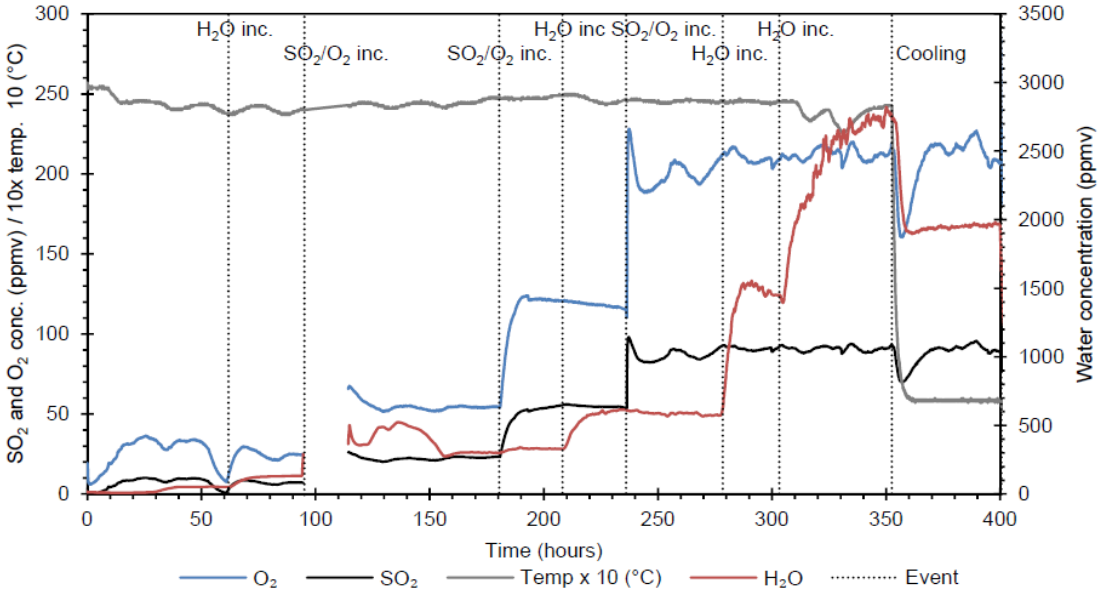

FIGURE 3. Analysis of the exhaust gas from Exp-01. The dashed lines indicate the time for change in temperature, water content or SO_2/O_2 content.

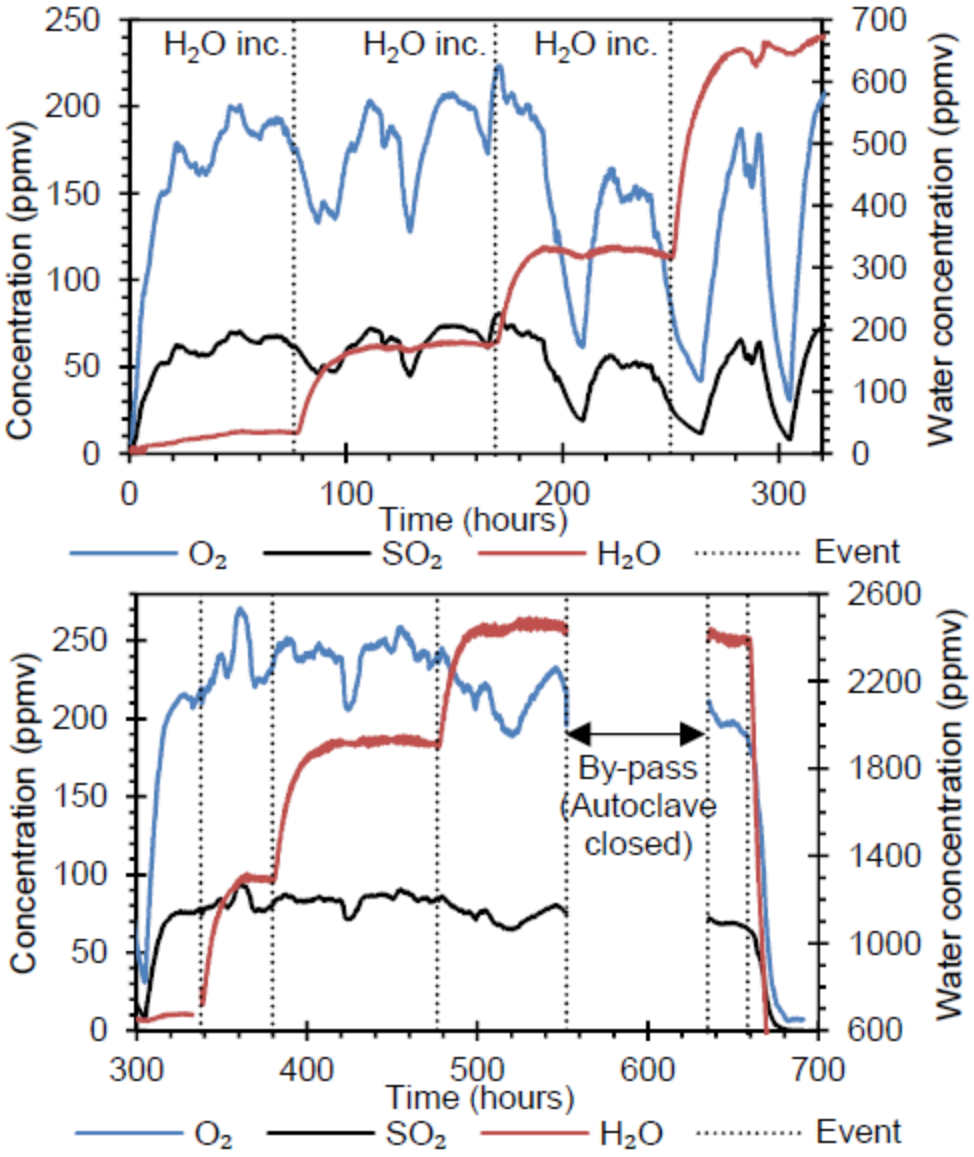

FIGURE 4. Analysis of exhaust gas from Exp-02. The dashed lines indicate events like change in water content or by-pass period.

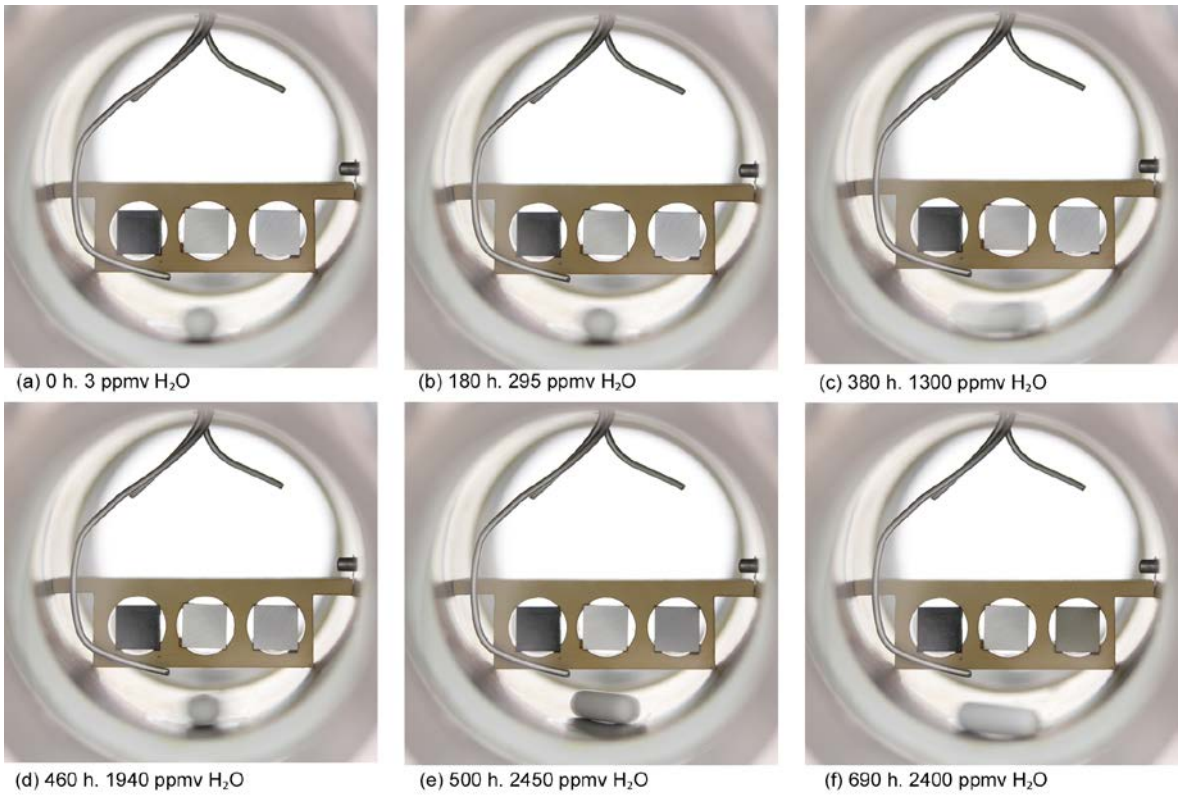

FIGURE 5. Still images from Exp-02. The left, middle, and right-hand side corrosion coupons were, respectively, carbon steel with mill scale, duplex steel, and polished carbon steel.

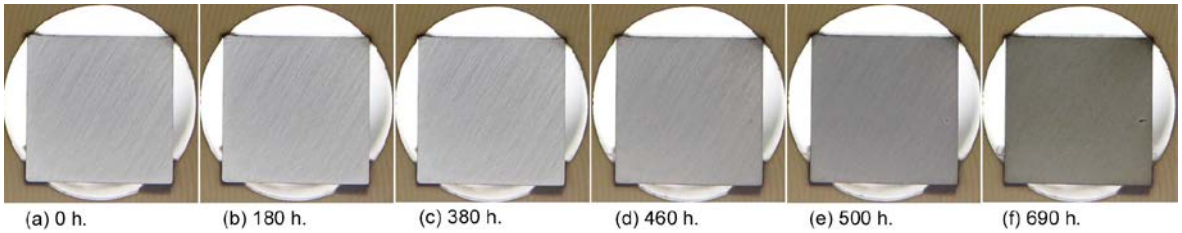

FIGURE 6. Enlargement of the polished carbon steel coupon from Figure 5 with time scale.

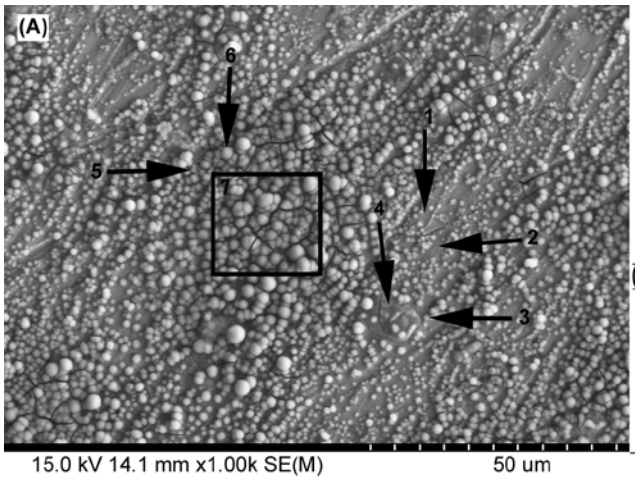

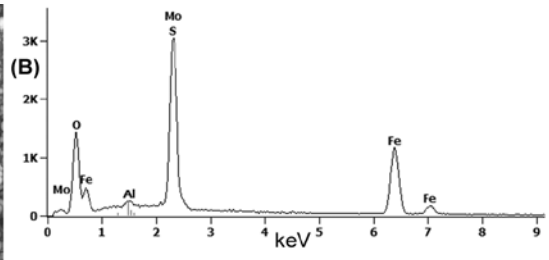

(C)	C-K	O-K	Al-K	S-K	Mn-K	Fe-K	Mo-L
pt1	3.5	14.6		2.1	0.6	78.4	0.7
pt2		22.4	1.2	3.3	0.7	71.7	0.7
pt3	3.7	16.2	1.1	2.1	0.5	75.7	0.7
pt4		63.4		15.3		21.4	
pt5		72.1	0.4	13.7		13.8	
pt6		60.0	0.6	16.4		22.9	0.1
pt7		59.0	0.4	15.1		25.3	0.1

FIGURE 7. (A) SEM picture and (B and C) EDS analysis (atomic %) of carbon steel coupon exposed in Exp-02.

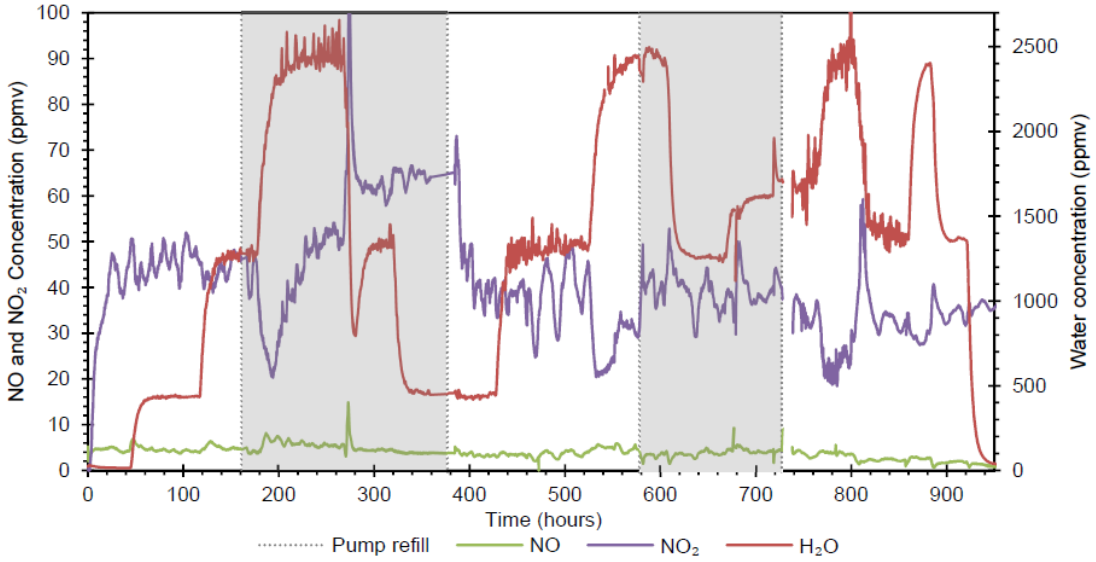

FIGURE 8. Analysis of exhaust gas in Exp-03. Periods with same impurity batch in the injection pump are indicated as white or light grey areas.

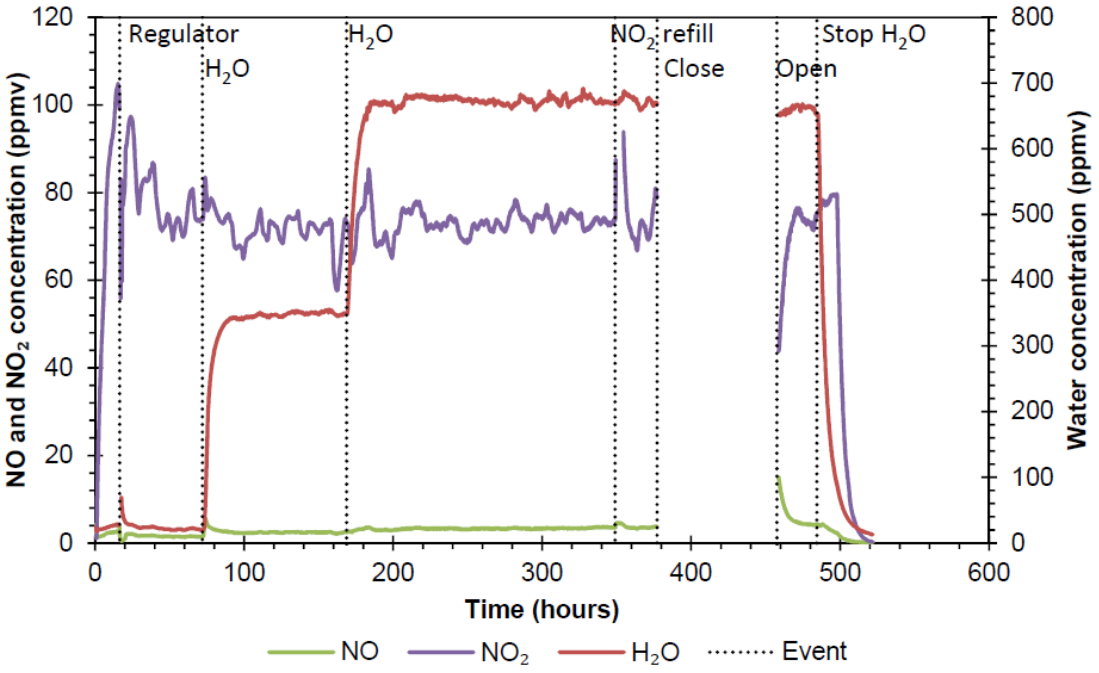

FIGURE 9. Analysis of exhaust gas in Exp-04. The dashed lines indicate the time for change in water content.

FIGURE 10. Still pictures from Exp-04. The left, center, and right-hand side corrosion coupons were, respectively, duplex stainless steel, carbon steel with mill scale, and polished carbon steel.

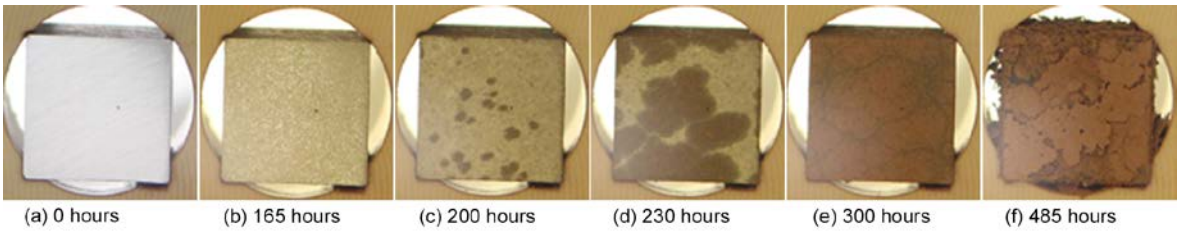

FIGURE 11. Enlargement of the carbon steel coupon in Figure 10 with time scale, exposed to 70 ppmv NO_2 and max. 670 ppmv water.

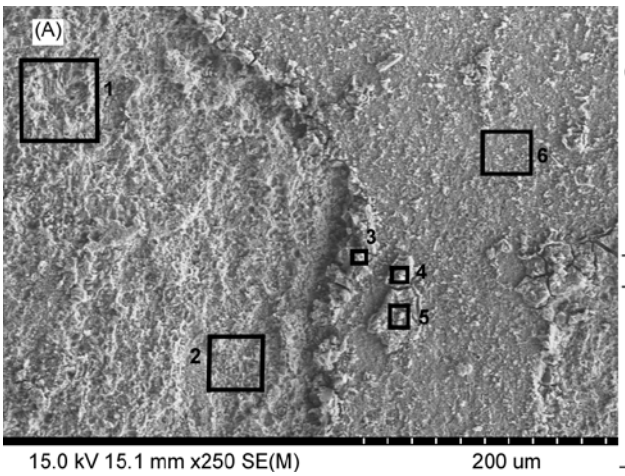

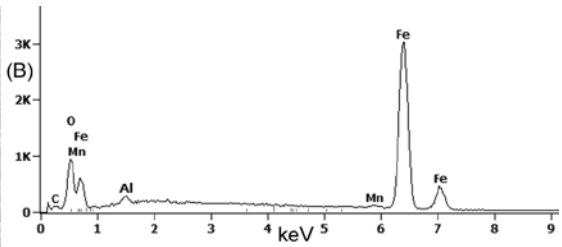

(C)	C-K	O-K	Al-K	Mn-K	Fe-K
pt1		41.3	1.2	0.6	56.9
pt2	3.6	35.4	1.1	0.6	59.3
pt3	2.5	69.8	0.5	0.3	26.9
pt4		64.1	0.8		35.1
Pt5		70.7	0.6	0.3	28.4
pt6	2.8	51.7	0.8	0.6	44.1

FIGURE 12. (A) SEM and (B, C) EDS analysis (atomic %) of carbon steel coupon exposed in Exp-04.

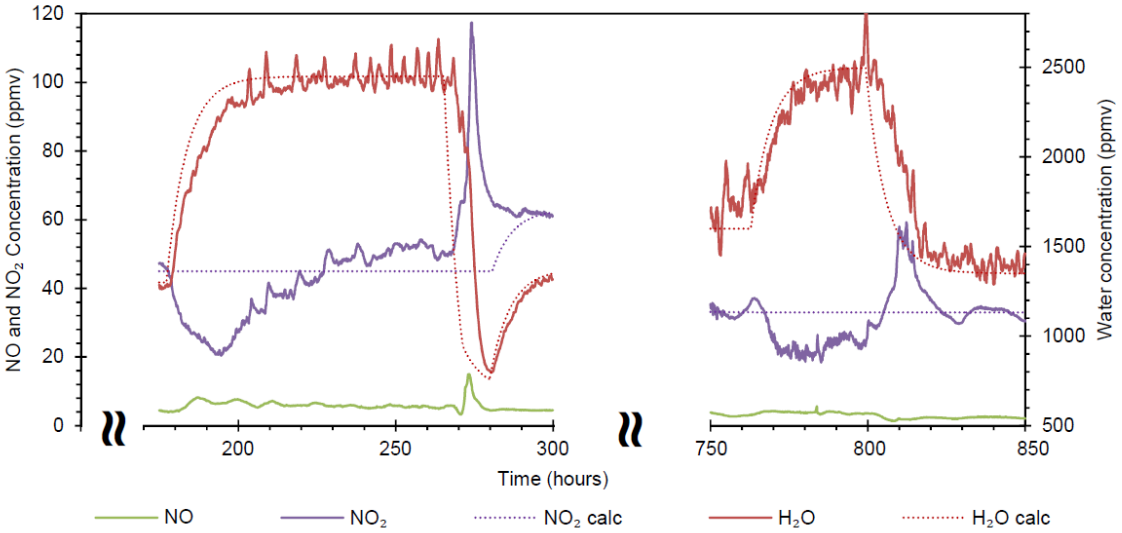

FIGURE 13. Extract from Figure 7 (Exp-03) showing the absorption and desorption of NO_2 with increasing and decreasing water concentration. The dashed lines are theoretical concentrations, made from mass balance calculations assuming that no chemical reactions occurred.

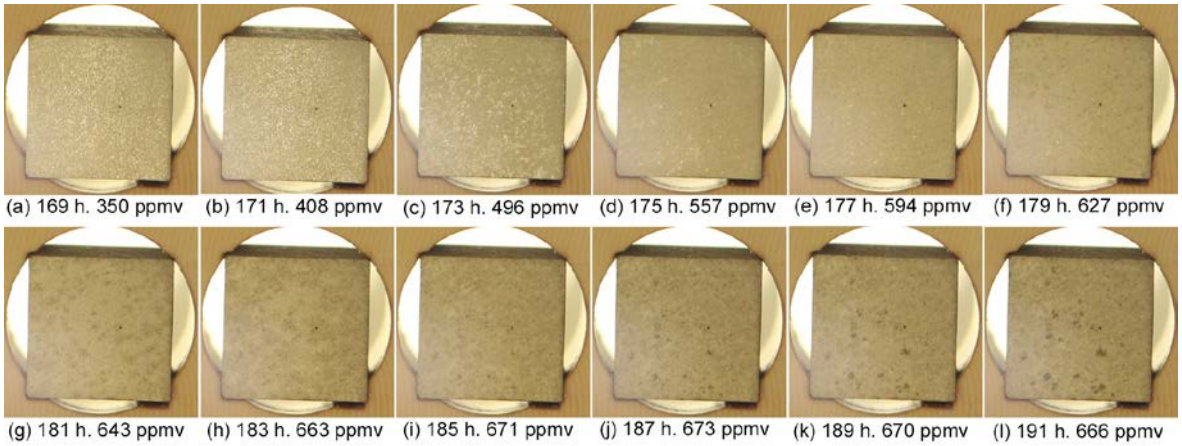

FIGURE 14. Exp-04; The carbon steel coupon exposed to NO_2 with increasing water concentration.

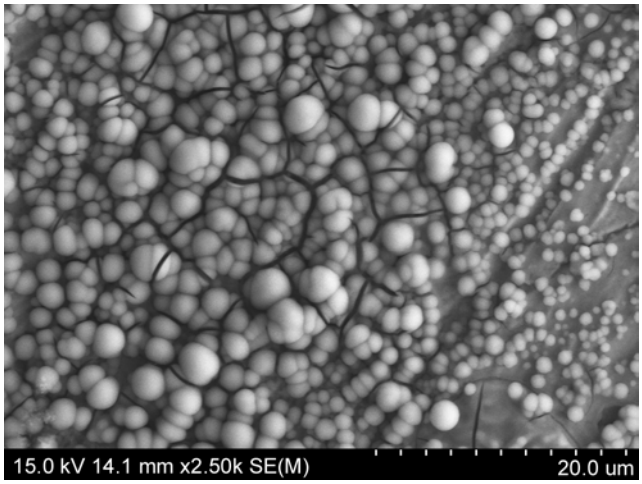

FIGURE 15. Close-up of Figure 6, showing spherical $FeSO_4$ products on the carbon steel surface.